HHS Public Access
Author manuscript
Ann Biomed Eng. Author manuscript; available in PMC 2020 May 12.

Published in final edited form as:
Ann Biomed Eng. 2018 March ; 46(3): 475–487. doi:10.1007/s10439-017-1960-z.

SpinoBot: An MRI-Guided Needle Positioning System for Spinal Cellular Therapeutics

Alexander Squires[1], **John N. Oshinski**[2,3], **Nicholas M. Boulis**[4], **Zion Tsz Ho Tse**[1,*]

[1]Engineering, The University of Georgia, Athens, GA,

[2]Radiology and Imaging Sciences, Emory University, Atlanta, GA;

[3]Biomedical Engineering, Georgia Institute of Technology & Emory University, GA;

[4]Neurosurgery, Emory University Hospital, Emory University School of Medicine, Atlanta, GA

Abstract

The neurodegenerative disease amyotrophic lateral sclerosis (ALS) results in the death of motor neurons in voluntary muscles. There are no cures for ALS and few available treatments. In studies with small animal models, injection of cellular therapeutics into the anterior horn of the spinal cord has been shown to inhibit the progression of ALS. It was hypothesized that spinal injection could be made faster and less invasive with the aid of a robot. The robotic system presented—SpinoBot—uses MRI guidance to position a needle for percutaneous injection into the spinal cord. With four degrees of freedom (DOF) provided by two translation stages and two rotational axes, SpinoBot proved capable of advanced targeting with a mean error of 1.12 mm and standard deviation of 0.97 mm in bench tests, and a mean error of 2.2 mm and standard deviation of 0.85 mm in swine cadaver tests. SpinoBot has shown less than 3% signal-to-noise ratio reduction in 3T MR imaging quality, demonstrating its compliance to the MRI environment. With the aid of SpinoBot, the length of the percutaneous injection procedure is reduced to less than 60 minutes with 10 minutes for each additional insertion. Although SpinoBot is designed for ALS treatment, it could potentially be used for other procedures that require precise access to the spine.

Key Terms

MRI-guided intervention; spinal injection; stem cell therapy; medical robotics; MRI compatible

Introduction

Amyotrophic lateral sclerosis (ALS) is a neurodegenerative disease that involves the gradual deterioration and eventual death of motor neurons. There are treatments that may slow the progression of ALS, but there is no cure. Most people with ALS die from respiratory failure, usually within 3 to 5 years from the onset of symptoms, according to the US National Institute of Neurological Disorders and Stroke[1]. Stem cell injection into the spinal cord could potentially be a cure. Literature on animal and phase I human clinical trial studies

---

[*]Corresponding Author: Zion Tsz Ho Tse; 597 D.W. Brooks Dr, Driftmier Engineering Center, Annex Room 111, Athens, GA 30602; ziontse@uga.edu; 706-542-4189.

Author Manuscript Author Manuscript Author Manuscript Author Manuscript

Author Manuscript Author Manuscript Author Manuscript Author Manuscript

indicates that injecting stem cells into the ventral horn of the spinal cord in proximity to the cervical enlargement results in axon regeneration and neuron re-myelination[4, 13, 14, 17, 37, 42].

The ventral horn of the spinal cord is located inside the vertebral column and is therefore surrounded by bony structures[2, 3]. The current clinical standard when transferring stem cells to the spinal cord is to perform a direct injection to the parenchyma of the spinal cord. Direct injection is used because migration of the stem cells to the target area is unnecessary and physicians have immediate visual confirmation that the cellular therapy has reached the intended location[24, 25, 30]. Performing a direct injection requires a surgery that removes the posterior portion of the vertebrae in order to gain access to the ventral horn of the spinal cord. In addition, the dura mater surrounding the spinal cord must be dissected for access to the cell delivery site[28, 41]. Because of the invasiveness of this multi-level laminectomy, it is only performed in trials with patients who are late in the progression of the disease[13].

To make this stem cell treatment more feasible to test and use on patients in the early stages of ALS, a less invasive approach is necessary. Percutaneous injection is a desirable alternative to open surgery because it is less invasive, reduces the risk of blood loss and injection, and decreases the time of hospitalization and patient recovery[41]. However, percutaneous access to the ventral horn without hitting the surrounding structures requires manipulation of both the needle location and orientation under image guidance in order to achieve the required trajectory for hitting the target. Therefore, the use of an image-guided needle targeting system is necessary to achieve percutaneous injections to the spine.

Presently, there are a number of image-guided needle positioning systems commercially available[5, 8, 23, 31, 35], and the majority of these systems are guided by ultrasound (US) or computed tomography (CT) because these imaging techniques offer good patient accessibility and streamlined workflow. However, for the treatment of ALS and other spinal injections, an MRI-guided approach is necessary because injections into the spinal cord should be administered into the gray matter for maximum effect. CT and US cannot detect the difference between gray matter and white matter, whereas MRI imaging can.

Magnetic resonance imaging (MRI) guided needle positioning systems have been reported in research and clinical settings[6, 10, 11, 15, 16, 19–21, 29, 33, 34, 39] and also highlighted in the MRI compatible robotics literature review[12], while only a few of them have been commercialized[22, 26, 27, 36, 38, 40]. To the authors’ best knowledge, none of them is specifically designed for spinal cord targeting.

We have developed SpinoBot, an MRI-guided robotic system that is capable of guiding precise percutaneous injections into the spinal cord. SpinoBot is designed to specifically address the issues found in the existing positioning models. The benefits SpinoBot will bring to the stakeholders are outlined in Table 1. The purpose of this device is to reduce the time of the procedure, lessen the invasiveness for the patient, and increase targeting accuracy within the spinal cord. Targeting accuracy is particularly important because the difference of a few degrees in targeting determines whether a needle slips between vertebrae or deflects off bone, particularly in smaller subjects. In this study, the advantages of SpinoBot as an MRI-guided needle positioning system for delivering cellular therapeutics to the spinal cord

Author Manuscript Author Manuscript Author Manuscript Author Manuscript

are examined. Although SpinoBot is designed for ALS treatment, it could potentially be used for other procedures that require precise access to the spine.

Materials and Methods

Design

Our aim was to design a device that assists physicians with achieving the desired needle trajectory into the spinal cord such that the ventral horn can be successfully targeted. The design specifications for SpinoBot, shown in Table 2, were obtained from consultations with the surgeons and MRI interventional radiologists on our team.

SpinoBot (Fig. 1b–e, Table 3) was designed to have a fully actuated 2 degree-of-freedom (DOF) translational positional platform, and a fully actuated 2 DOF angular end effector for needle positioning. This system provides sub-degree angulation adjustments. Once the needle is in place, the physician manually performs the needle insertion.

In order to position the needle in the desired location in the horizontal plane of the robot, two motors are used to move the needle guide. One motor (part 2 in Fig.1b) is used for translation in the left-to-right direction, and the second motor (part 3 in Fig.1b) is used for translation in the head-to-foot direction. Similarly, in order to angle the needle as desired, two motors (parts 5 & 6 in Fig.1b) are used to rotate the needle guide about the left-to-right axis and the head-to-foot axis. The needle channel is designed to be non-backdrivable so SpinoBot can act as a rigid needle guide for needle insertion into the vertebrae. This is achieved by using a high gear ratio of 2000:1 in the planetary gear transmission between the pneumatic motor drive and the needle channel.

The primary design hurdle of the angulation stage was fitting a pair of motor and gearbox combinations in the space available (Fig. 1). The ultimate solution to volume constraints was inspired by the CoreXY system and mechanical differentials[21]. The developed angulation stage uses a pair of fixed motors to attain rotation in two planes, with head-to-foot rotation (θ) of ±35° and left-to-right rotation (φ) of ±30°. The angulation units of the angulation stage pivot on the large hub of the input gears. The needle guide rotates within the phi angulation unit on an axis perpendicular to that of the theta angulation unit.

The control of two rotational axes via a pair of linked input motors is due to the symmetry of the gear system about the miter gear, which is attached to the needle guide. The rotation of one input while the other remains fixed results in the rotation of both the angulation units and the needle guide; action by both motors allows control of rotation about both axes (Figs. 1d, 2). Rotation of the inputs in the same direction causes opposing forces to be applied to the gear attached to the needle guide, negating its rotation. These forces result in the rotation of the angulation units. If the inputs are rotated in opposite directions, forces act cooperatively to rotate the needle guide, and no action is applied to the floating guide. With miter gears joined directly to the input shafts and the needle guide, the following simple equations define rotations in the θ and φ planes using input motor rotations, angles R_1 and R_2, reduced through a gear ratio of G_r. d denotes the differential of each parameter:

Author Manuscript

Author Manuscript

Author Manuscript

Author Manuscript

$$d\theta = \frac{dR_1 + dR_2}{2G_r}$$

$$d\varphi = \frac{dR_1 - dR_2}{2G_r}$$

However, appropriately sized miter or bevel gears could not be sourced to fit within the limited volume of the angulation stage while maintaining the required angulation capabilities. Instead, timing belts were used along with smaller miter gears between the inputs and the needle guide, adding the timing pulley ratio G_b to the calculation of φ:

$$d\varphi = \frac{dR_1 - dR_2}{2G_rG_b}$$

Registration and Targeting

A total of seven fiducial markers (Beekley® PinPoints, 6 mm diameter spheres) are embedded in SpinoBot. Four are used to register SpinoBot to the MR coordinate system. This is achieved by entering the known coordinates of the center of the markers into custom trajectory calculation software (programmed in LabVIEW). A transformation matrix is determined by comparing the MRI coordinates of the fiducial markers to the known positions of the fiducials in the robot coordinate system. Another fiducial marker is used to determine the left and right orientation of SpinoBot relative to the patient.

The use of a continuous end effector for rotation required adding angulation calculation to the robot registration to ensure the needle guide is in the right orientation so that the needle is aligned with the target. Angulation calculation was accomplished by embedding two additional fiducial markers along the needle channel at two known points. The locations of the fiducials for coordinate registration were placed between the subject and the needle guide to ensure their visibility in any imaging sequence which captured both the needle guide and the subject. With an actuated rotational stage, the angle specified by the target and path points could be met within the workspace.

Made of plastic, the guide itself is invisible in MR images. Visualization of the needle guide is made possible by empty space in the form of a cylindrical shell surrounding the guidance channel. To ensure visibility, this space was filled with fluid extracted from the same fiducial markers that were used for registration.

While the calculation of targeting angles based on the two points selected by the operator remains the default method of angle selection, a second targeting option in the form of operator-defined angles was added at the request of end users. The selection of a path point is replaced by the explicit definition of θ and φ by the operator. A removable manual protractor to assist in this process was added to the floating stage. This protractor could be used to define θ and φ even without registration, and to verify the insertion angle and further adjust if necessary before insertion.

Author Manuscript

Author Manuscript

Author Manuscript

Author Manuscript

Control Strategy to Minimize Transmission Backlash

Testing of the system presented errors caused by the deviation of the actual gear trains and belt systems from the idealized system. Gear backlash and fractionally mistightened timing belts create a situation wherein a motor effectively jumps ahead of the end effector upon reversing. This jump is caused by a loss of motion as the gear train and belts reverse into the backlash opposite the previous direction of actuation.

This issue was addressed in two ways. First, the end stage of the miter gear was fabricated in-house with very high precision to minimize the backlash of the overall system. Second, a buffer was established on each axis which accounted for the backlash upon reversing direction (Fig. 3). The primary role of the buffer system was to reduce the backlash in the 2000:1 planetary gearbox attached to the pneumatic motor drive. Because the gearbox has a large gear ratio and multiple stages of planetary gears, reducing backlash in this component was key to reducing the overall error of the system.

The input (dC_{in}) to each buffer was the count from the quadrature encoder on a motor; the output (dC_{out}) was a modified count which was used to update the robot position. The buffer value (B_n) from the previous loop was updated by the motor quadrature count in the current loop:

$$B_{n+1} = B_n + dC_{in}$$

If the resulting value of B_{n+1} is greater than B_{max} or less than 0, an output value dC_{out} is calculated; if B_{n+1} falls between 0 and B_{max}, dC_{out} is 0:

$$if\ B_{n+1} > B_{max} : dC_{out} = B_{n+1} - B_{max}$$

$$else\ if\ B_{n+1} < 0 : dC_{out} = B_{n+1}$$

$$else : dC_{out} = 0$$

The value of B_{max} was determined empirically by tracking the lost distance or angle with an NDI Aurora V2 Electromagnetic Tracking System and converting the result to a quadrature count. The final step is to set the buffer value to within the range of $[0, B_{max}]$ before passing it to the next loop:

$$B_{n+1} = \max(0, \min(B_{n+1}, B_{max}))$$

The final component of the control strategy was to implement a verification step in the clinical workflow. In this step, an MRI scan is taken to ensure the correct needle channel orientation and position after the robot moves the needle channel to align with the targeted trajectory and right before the needle insertion. If a positioning error is observed in the scan,

Author Manuscript Author Manuscript Author Manuscript Author Manuscript

the robotic system will be recalibrated and repositioned to ensure no accumulative error has occurred.

Bench Tests

Bench testing based on ASTM F2554–10[18] was performed to validate the targeting accuracy between the actual and the desired targets of the 4 DOF system in three tests using the NDI Aurora V2 Electromagnetic Tracking System and a 3D-printed geometric phantom. The phantom used in this study was an array of pyramid structures with well-defined geometric targets, which was 3D-printed using ABS thermoplastic (acrylonitrile butadiene styrene). The robot was mounted on top of the phantom and a number of target points were chosen (each target point was one of the pyramid peaks, selected from the array of pyramids). The robot was controlled to target those points. This was possible because we 3D-printed the pyramids with high accuracy so the coordinates of the pyramid peaks are known. After the robot aligned the needle channel with a target point, an electromagnetically tracked needle was inserted to the predefined depth and the ETS provided us with the position of the needle, which we compared with the target point position to determine the error based on the ISO1101 standard[32].

Test 1. The first test (n=40) maintained a fixed orientation of the rotation stage in order to test the XY stage accuracy.

Test 2. The rotation stage was tested to confirm rotation accuracy. Angles were obtained as the needle guide was rotated and compared to the reported position (n=40).

Test 3. 4DOF system tests were performed, combining both translation and rotation. Target points on the geometric phantom were selected and measured using the electromagnetic tracker, and the robot was positioned according to the targeting calculations. Then the error between the desired and the actual needle tip position was measured.

Compliance to 3T MRI environment

SpinoBot was tested for MRI compliance in a 3T Siemens MRI scanner using the following steps:

1. A container was filled with CuSO4 solution (1.25 g/l concentration). This container was placed in the MRI bore and scanned with a TSE (turbo spin echo) sequence and a True FISP (fast imaging with steady-state precession) sequence. Images were saved in DICOM format. The images of the container were used as the experimental control. The TSE and True FISP sequence parameters were held constant throughout MRI compliance testing.
2. SpinoBot was disconnected from the power source and placed next to the geometric phantom used in the bench tests. The phantom was scanned with the same imaging sequences used in step 1.
3. SpinoBot was connected to the power source, but kept at rest, and placed next to the geometric phantom used in the bench tests. The phantom was scanned with the same imaging sequences used in step 1.

Author Manuscript

Author Manuscript

Author Manuscript

Author Manuscript

4. SpinoBot was connected to the power source, and operated with all 4 DOF in full motion, and placed next to the geometric phantom used in the bench tests. The phantom was scanned with the same imaging sequences used in step 1.

5. The signal-to-noise ratio (SNR) of each image was calculated using the following equation:

$$SNR = \frac{P_{center}}{SD_{corner}}$$

   where P_{center} is the mean signal of a 40 × 40 pixel region at the center of the image and SD_{corner} is the standard deviation of the signal of a 40 × 40 pixel region at the corner of the image. Theoretically, any signal at the corner of the control image outside of the phantom boundary is caused only by noise. The change in SNR between variable and control images was calculated by subtracting the SNR value of the corresponding control image from the variable image.

Swine Cadaver Tests

A 35 lb swine cadaver was used to evaluate the functionality of SpinoBot in a 3.0 Tesla MRI scanner (MAGNETOM Prisma Fit, Siemens Medical) at the Emory University Center for Systems Imaging (Fig. 4). The cadaver was secured inside a plastic container and SpinoBot attached above the cervical spine. After covering the exposed portions of the cadaver, a body coil was placed over the supporting bars of the robot. After localizing the subject, a high-resolution image (3D, magnetization-prepared, T1-weighted (T1w) fast gradient echo sequence (MP RAGE)), containing anatomy and the registration fiducial markers was obtained. Two points along the needle trajectory were selected by the surgeon. One point is the target point in the ventral horn. The other point is a point (between the vertebrae) through which the needle will pass before reaching the target point. After aligning the needle guide for each insertion, a small incision was made using an MR-safe scalpel where the needle contacted the skin. The needle was then inserted to the prescribed depth. A confirmation scan (T2*-weighted gradient echo sequence) visualized the needle after each insertion. Gadolinium was injected into the spine after the first insertion to visualize the affected area. Fifteen total insertions were performed.

Results

System Calibration

Comparison of translation positioning accuracy with and without implementation of the buffering system is shown in Fig. 5. The x-axis is the target position (which is the position defined by the user for the needle to target), and the y-axis is the difference between the target position and the measured position of the needle (which is the position reached by the tip of the needle and measured). Prior to implementation of the buffer, systemic positioning errors were observed when back-forth motion occurred and created transmission backlash. Implementation of the buffer reduced the systemic error to a negligible level, as supported by a two-sample t-test (p=0.61).

Author Manuscript
Author Manuscript
Author Manuscript
Author Manuscript

Bench Tests

Test 1: The translation error mean after the inclusion of the positioning buffer was μ = 0.04 mm, and the standard deviation was **σ** = 0.09 mm. Measurement resolution was 0.7 mm.

Test 2: Rotation accuracy performed with a mean error of 0.6° and a standard deviation of 0.3°.

Test 3: Full system bench tests returned a positioning error within acceptable levels (μ = 1.12 mm, **σ** = 0.97 mm).

Compliance to 3T MRI environment

The maximum SNR reduction in the MR image quality was 2.7% with the TSE sequence, and 2.9% with the True FISP sequence. The images of the phantom taken with the True FISP sequence in different scan conditions, and the corresponding SNR reduction percentages, are shown in Fig. 6. SNR reduction values under all conditions are within the acceptable level of 10% proposed by Chinzei[7]. Therefore, the MRI compliance test results indicate decent compatibility of SpinoBot with the MR environment.

Swine Cadaver Tests

In cadaver trials, MRI-guided insertions into the spine were performed with a mean accuracy of 2.2 mm and standard deviation of 0.85 mm for successful insertions. Fig. 7 provides an example of a successful insertion. Table 4 outlines the procedural steps, and length of time for each step, of spinal injection using SpinoBot. The first insertion took less than 60 minutes, and each additional insertion took another 10 minutes.

Discussion

SpinoBot assists physicians with needle positioning for percutaneous injection into the spinal cord under MRI guidance, which is a less invasive option than multilevel laminectomy (the conventional open surgery procedure for spinal cord access). The robotic system has been shown to be MRI conditional (SNR reduction of <3%), allowing for accurate targeting of the ventral horn of the spinal cord under MRI guidance. Design requirements were specified by neurosurgeons and interventional radiologists to ensure that the system meets clinical standards.

The ventral horn is difficult to target since it is surrounded by vertebrae, so SpinoBot is designed to guide the needle to specific target locations with continuous targeting selection and high targeting resolution. The motorized system enables precise translational and angular needle positioning, providing the maneuverability required to reach ventral horn targets of the spinal cord. The continuous angulation and translation improves the ability to avoid vertebrae, significantly enabling accuracy targeting, as half of a millimeter can be the difference between successful targeting and grazing the bone, causing needle trajectory deflection.

The SpinoBot system has been tested for targeting accuracy of spinal cord injections under MRI guidance. In bench tests, the mean targeting error was 1.12 mm with standard deviation

Author Manuscript Author Manuscript Author Manuscript Author Manuscript

of 0.97 mm, and in swine cadaver tests, the mean targeting error was 2.2 mm with standard deviation of 0.85 mm. The procedural workflow was also evaluated in the swine cadaver tests. The first insertion took less than 60 minutes, and each additional insertion took another 10 minutes. Once the first set of coordinates has been targeted (steps 3, 4, and 5 in Table 4), targeting a new set of coordinates is quick because the operator can plan the subsequent insertion during the confirmation scans. According to our results, MRI-guided procedures using SpinoBot for spinal cord targeting are possible.

Future work will focus on the following considerations. First, improving the manufacturing method would improve the final product; currently, SpinoBot is manufactured using 3D printing, but precise milling techniques would reduce the clearance between the needle and guidance holes. Second, implementing a motorized insertion axis could potentially reduce targeting errors related to patient movements and mis-registration, as well as shorten the procedure time.

Acknowledgments

This study was supported in part by the National Institutes of Health (NIH) Bench-to-Bedside Award, the NIH Center for Interventional Oncology Grant, the National Science Foundation (NSF) I-Corps Team Grant (1617340), NSF REU site program 1359095, the UGA-AU Inter-Institutional Seed Funding, the American Society for Quality Dr. Richard J. Schlesinger Grant, the PHS Grant UL1TR000454 from the Clinical and Translational Science Award Program, and the NIH National Center for Advancing Translational Sciences. The authors declare that they have no conflicts of interest.

References

1. Amyotrophic Lateral Sclerosis (ALS) Information Page. NIH National Institute of Neurological Disorders and Stroke.
2. Anatomy Gross. Memorang.
3. An Overview of the Central Nervous System : The Spinal Cord HumanPhysiology.Academy, 2014.
4. Asheuer M, Pflumio F, Benhamida S, Dubart-Kupperschmitt A, Fouquet F, Imai Y, Aubourg P and Cartier N. Human CD34+ cells differentiate into microglia and express recombinant therapeutic protein. Proc Natl Acad Sci USA 101: 3557–3562, 2004. [PubMed: 14990803]
5. Bertelsen A, Melo J, Sánchez E and Borro D. A review of surgical robots for spinal interventions. Int J Med Robot 9: 407–422, 2013. [PubMed: 23239581]
6. Chinzei K, Hata N, Jolesz FA and Kikinis R. MR compatible surgical assist robot: System integration and preliminary feasibility study In: International Conference on Medical Image Computing and Computer-Assisted InterventionSpringer, 2000, p. 921–930.
7. Chinzei K, Kikinis R and Jolesz FA. MR compatibility of mechatronic devices: design criteria In: Medical Image Computing and Computer-Assisted Intervention– MICCAI’99Springer, 1999, p. 1020–1030.
8. Cleary K, Melzer A, Watson V, Kronreif G and Stoianovici D. Interventional robotic systems: Applications and technology state‐ of-the-art. Minim Invasive Ther Allied Technol 15: 101–113, 2006. [PubMed: 16754193]
9. Elhawary H, Tse ZTH, Hamed A, Rea M, Davies BL and Lamperth MU. The case for MR-compatible robotics: a review of the state of the art. Int J Med Robot 4: 105–113, 2008. [PubMed: 18481822]
10. Elhawary H, Zivanovic A, Rea M, Davies BL, Besant C, Young I and Lamperth M. A modular approach to MRI-compatible robotics. IEEE Eng Med Biol Mag 27: 35–41, 2008. [PubMed: 18519180]

Author Manuscript Author Manuscript Author Manuscript Author Manuscript

11. Fischer GS, Iordachita I, Csoma C, Tokuda J, DiMaio SP, Tempany CM, Hata N and Fichtinger G. MRI-compatible pneumatic robot for transperineal prostate needle placement. IEEE ASME Trans Mechatron 13: 295–305, 2008. [PubMed: 21057608]
12. Gassert R, Burdet E and Chinzei K. MRI-compatible robotics. IEEE Eng Med Biol Mag 27: 12–14, 2008.
13. Glass JD, Boulis NM, Johe K, Rutkove SB, Federici T, Polak M, Kelly C and Feldman EL. Lumbar Intraspinal Injection of Neural Stem Cells in Patients with Amyotrophic Lateral Sclerosis: Results of a Phase I Trial in 12 Patients. Regen Med 30: 1144–1151, 2012.
14. Goolsby J, Marty MC, Heletz D, Chiappelli J, Tashko G, Yarnell D, Fishman PS, Dhib-Jalbut S, Bever CT Jr., Pessac B and Trisler D. Hematopoietic progenitors express neural genes. Proc Natl Acad Sci USA 100: 14926–14931, 2003. [PubMed: 14634211]
15. Hempel E, Fischer H, Gumb L, Höhn T, Krause H, Voges U, Breitwieser H, Gutmann B, Durke J and Bock M. An MRI-compatible surgical robot for precise radiological interventions. Comput Aided Surg 8: 180–191, 2003. [PubMed: 15360099]
16. Ho M, McMillan AB, Simard JM, Gullapalli R and Desai JP. Toward a meso-scale SMA-actuated MRI-compatible neurosurgical robot. IEEE Trans Robot 28: 213–222, 2012.
17. Hoehn M, Kustermann E, Blunk J, Wiedermann D, Trapp T, Wecker S, Focking M, Arnold H, Hescheler J, Fleischmann BK, Schwindt W and Buhrle C. Monitoring of implanted stem cell migration in vivo: a highly resolved in vivo magnetic resonance imaging investigation of experimental stroke in rat. Proc Natl Acad Sci USA 99: 16267–16272, 2002. [PubMed: 12444255]
18. International A. ASTM F2554–10, Standard Practice for Measurement of Positional Accuracy of Computer Assisted Surgical Systems. West Conshohocken, PA: 2010.
19. Krieger A, Iordachita II, Guion P, Singh AK, Kaushal A, Ménard C, Pinto PA, Camphausen K, Fichtinger G and Whitcomb LL. An MRI-compatible robotic system with hybrid tracking for MRI-guided prostate intervention. IEEE Trans Biomed Eng 58: 3049–3060, 2011. [PubMed: 22009867]
20. Krieger A, Song S-E, Cho NB, Iordachita II, Guion P, Fichtinger G and Whitcomb LL. Development and evaluation of an actuated MRI-compatible robotic system for MRI-guided prostate intervention. IEEE ASME Trans Mechatron 18: 273–284, 2013.
21. Krieger A, Susil RC, Ménard C, Coleman JA, Fichtinger G, Atalar E and Whitcomb LL. Design of a novel MRI compatible manipulator for image guided prostate interventions. IEEE Trans Biomed Eng 52: 306–313, 2005. [PubMed: 15709668]
22. Lacey C and Sutherland G. Advancing neurosurgery through translational research. Neurosurgery 72 Suppl 1: 176–181, 2013. [PubMed: 23254806]
23. Maderer J and Feeney M. Putting the Right Face on an Assistive Robot. Biomed Saf Stand 44: 113–114, 2014.
24. Mazzini L, Ferrero I, Luparello V, Rustichelli D, Gunetti M, Mareschi K, Testa L, Stecco A, Tarletti R, Miglioretti M, Fava E, Nasuelli N, Cisari C, Massara M, Vercelli R, Oggioni GD, Carriero A, Cantello R, Monaco F and Fagioli F. Mesenchymal stem cell transplantation in amyotrophic lateral sclerosis: A Phase I clinical trial. Exp Neurol 223: 229–237, 2010. [PubMed: 19682989]
25. Mazzini L, Mareschi K, Ferrero I, Miglioretti M, Stecco A, Servo S, Carriero A, Monaco F and Fagioli F. Mesenchymal stromal cell transplantation in amyotrophic lateral sclerosis: a long-term safety study. Cytotherapy 14: 56–60, 2012. [PubMed: 21954839]
26. Melzer A, Gutmann B, Remmele T, Wolf R, Lukoscheck A, Bock M, Bardenheuer H and Fischer H. INNOMOTION for percutaneous image-guided interventions: principles and evaluation of this MR- and CT-compatible robotic system. IEEE Eng Med Biol Mag 27: 66–73, 2008.
27. Mert A, Gan LS, Knosp E, Sutherland GR and Wolfsberger S. Advanced cranial navigation. Neurosurgery 72 Suppl 1: 43–53, 2013. [PubMed: 23254812]
28. Papagelopoulos PJ, Peterson HA, Ebersold MJ, Emmanuel RP, Choudhury SN and Quast LM. Spinal Column Deformity and Instability After Lumbar or Thoracolumbar Laminectomy for Intraspinal Tumors in Children and Young Adults. Spine 22: 442–451, 1997. [PubMed: 9055374]
29. Pappafotis N, Bejgerowski W, Gullapalli R, Simard JM, Gupta SK and Desai JP. Towards design and fabrication of a miniature MRI-compatible robot for applications in neurosurgery In: ASME

Author Manuscript

Author Manuscript

Author Manuscript

Author Manuscript

2008 International Design Engineering Technical Conferences and Computers and Information in Engineering ConferenceAmerican Society of Mechanical Engineers, 2008, p. 747–754.

30. Riley J, Federici T, Polak M, Kelly C, Glass J, Raore B, Taub J, Kesner V, Feldman EL and Boulis NM. Intraspinal stem cell transplantation in amyotrophic lateral sclerosis: a phase I safety trial, technical note, and lumbar safety outcomes. Neurosurgery 71: 405–416; discussion 416, 2012. [PubMed: 22565043]
31. Ringel F, Ingerl D, Ott S and Meyer B. VARIOGUIDE: A NEW FRAMELESS IMAGE- GUIDED STEREOTACTIC SYSTEM—ACCURACY STUDY AND CLINICAL ASSESSMENT. Neurosurgery 64: ons365–ons373, 2009.
32. Standardization I. O. f. ISO 1101:2017 Geometrical product specifications (GPS) -- Geometrical tolerancing -- Tolerances of form, orientation, location and run-out. 2017.
33. Stoianovici D, Song D, Petrisor D, Ursu D, Mazilu D, Mutener M, Schar M and Patriciu A. “MRI Stealth” robot for prostate interventions. Minim Invasive Ther Allied Technol 16: 241–248, 2007. [PubMed: 17763098]
34. Sutherland GR, Latour I and Greer AD. Integrating an image-guided robot with intraoperative MRI. IEEE Eng Med Biol Mag 27: 59–65, 2008. [PubMed: 18519183]
35. Sutherland GR, McBeth PB and Louw DF. NeuroArm: an MR compatible robot for microsurgery. Int Congr Ser 1256: 504–508, 2003.
36. Sutherland GR, Wolfsberger S, Lama S and Zarei-nia K. The evolution of neuroArm. Neurosurgery 72 Suppl 1: 27–32, 2013.
37. Taguchi A, Soma T, Tanaka H, Kanda T, Nishimura H, Yoshikawa H, Tsukamoto Y, Iso H, Fujimori Y, Stern DM, Naritomi H and Matsuyama T. Administration of CD34+ cells after stroke enhances neurogenesis via angiogenesis in a mouse model. J Clin Invest 114: 330–338, 2004. [PubMed: 15286799]
38. Tan N, Lin W-C, Khoshnoodi P, Asvadi NH, Yoshida J, Margolis DJ, Lu DS, Wu H, Sung KH and Lu DY. In-Bore 3-T MR-guided Transrectal Targeted Prostate Biopsy: Prostate Imaging Reporting and Data System Version 2–based Diagnostic Performance for Detection of Prostate Cancer. Radiology 152827, 2016.
39. Tsekos NV, Yacoub E, Tsekos PV and Koutlas IG. Design of an MRI-compatible robotic stereotactic device for minimally invasive interventions in the breast. J Biomech Eng 126: 458–465, 2004. [PubMed: 15543863]
40. Wolter K, Decker G and Willinek W. Transperineal MR-guided stereotactic prostate biopsy utilizing a commercially available anorectal biopsy device In: RöFo-Fortschritte auf dem Gebiet der Röntgenstrahlen und der bildgebenden Verfahren© Georg Thieme Verlag KG, 2013, p. 116–120.
41. Yasuoka S, Peterson HA and MacCarty CS. Incidence of spinal column deformity after multilevel laminectomy in children and adults. J Neurosurg 57: 441–445, 1982. [PubMed: 7108592]
42. Zhao ZM, Li HJ, Liu HY, Lu SH, Yang RC, Zhang QJ and Han ZC. Intraspinal transplantation of CD34+ human umbilical cord blood cells after spinal cord hemisection injury improves functional recovery in adult rats. Cell Transplant 13: 113–122, 2004. [PubMed: 15129757]

Author Manuscript

Author Manuscript

Author Manuscript

Author Manuscript

(a) System overview

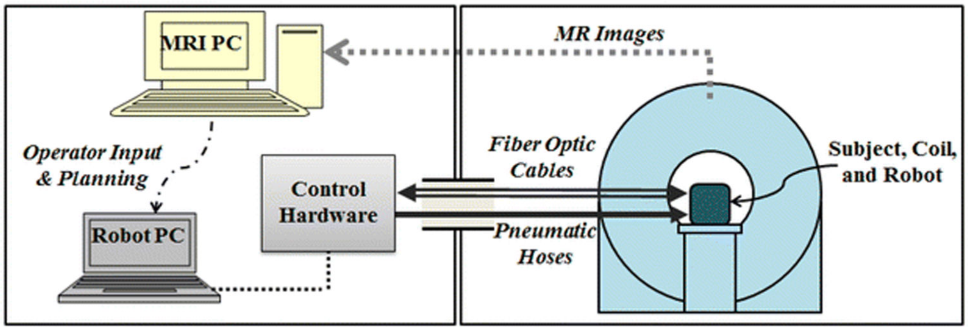

(b) CAD design **(c)** Assembled SpinoBot

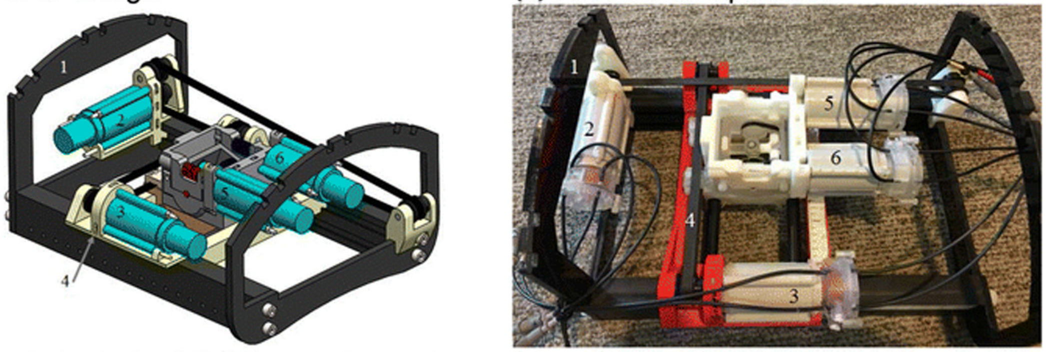

(d) Actuated 2-DOF rotation stage (shown as gray in (b)) **(e)** Contrast for needle guide visualization (bottom view of (d))

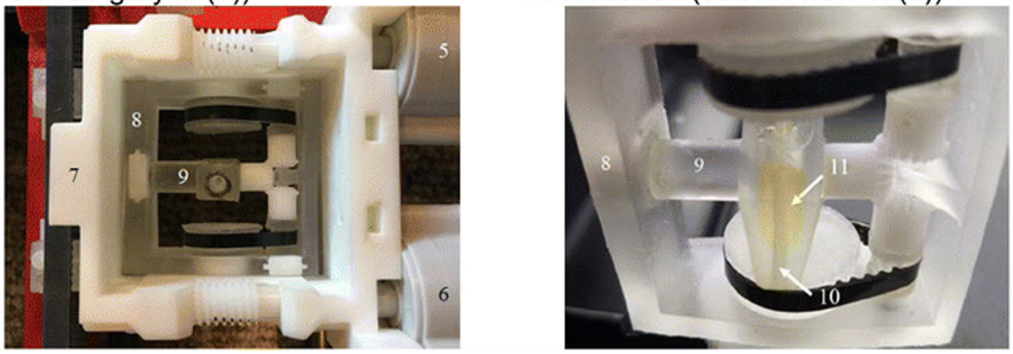

Figure 1.

(a) Block diagram overview of robotic system and its setup in MRI and control rooms. (b) CAD assembly of the 4DOF SpinoBot. (c) The assembled SpinoBot. (d) Close-up of the actuated rotation stage. (e) Close-up of needle guide. The following components are visible in (b) and (c): (1) coil support, (2) x-axis actuator, (3) y-axis actuator; (2) and (3) are connected to (4) translating stage. (d) and (e) show: (5,6) angulation actuators, which are connected to (7) angulation stage. (8) theta (θ) angulation unit allowing rotation in 2 DOF (See Fig. 2 for details), (9) phi (φ) angulation unit. Embedded in (9) is (10) a needle insertion guide containing (11) gadolinium image contrast agent (yellow fluid) for needle guide visualization.

Author Manuscript

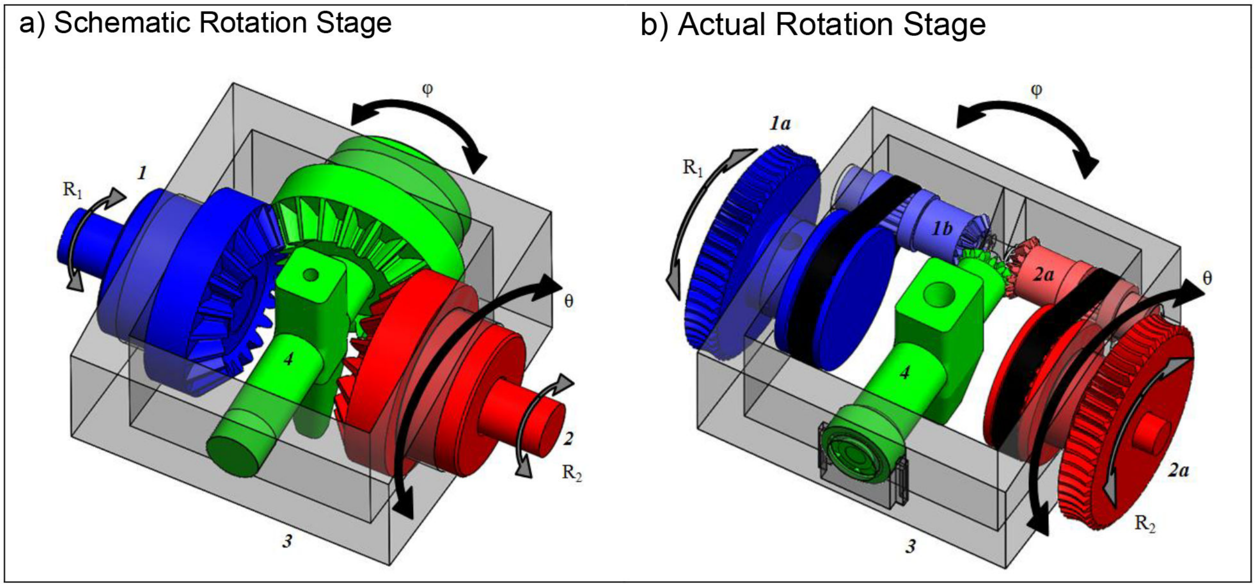

Figure 2.

CAD drawing of the motorized rotation stage. (a) The schematic configuration involves two input shafts (1, 2) driving a configuration of three miter gears, providing rotational motions θ and φ. Both θ and φ rotational directions are perpendicular to each other. Rotation in the θ direction (the theta angulation unit, 3) occurs when R1 and R2 rotate in the same direction. Rotation in the φ direction (phi angulation unit and needle insertion guide, 4) occurs when they rotate in opposing directions. (b) The actual design obeys the same relations, but utilized a timing belt in addition to miter gears to increase the workspace of the needle guide.

Author Manuscript Author Manuscript Author Manuscript Author Manuscript

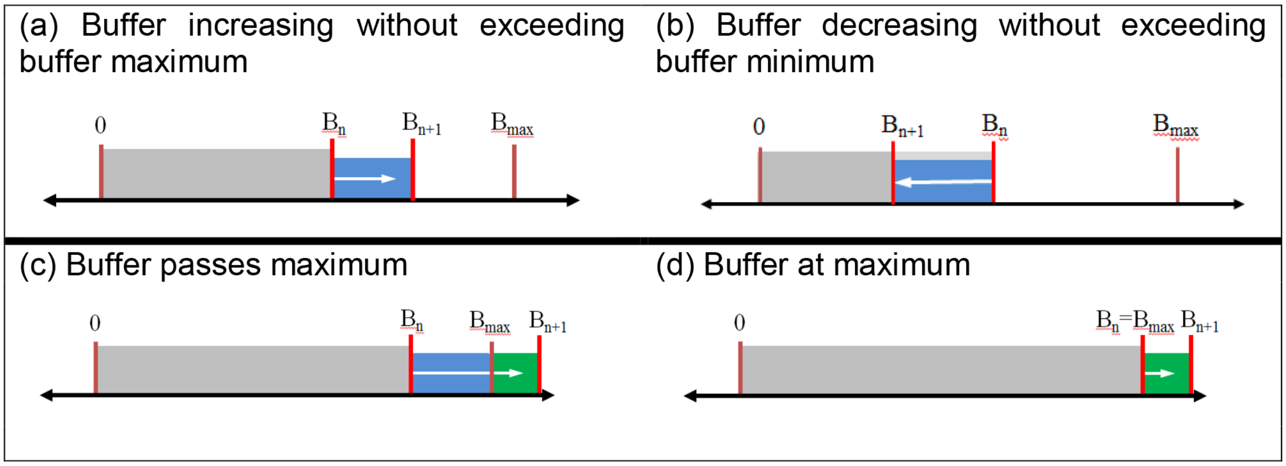

Figure 3.

Visual representation of the count buffering system. In situations (a) and (b), B_{n+1} falls between 0 and B_{max}. In (c), B_{n+1} exceeds B_{max}. In (d) the buffer limit has been reached.

Author Manuscript Author Manuscript Author Manuscript Author Manuscript

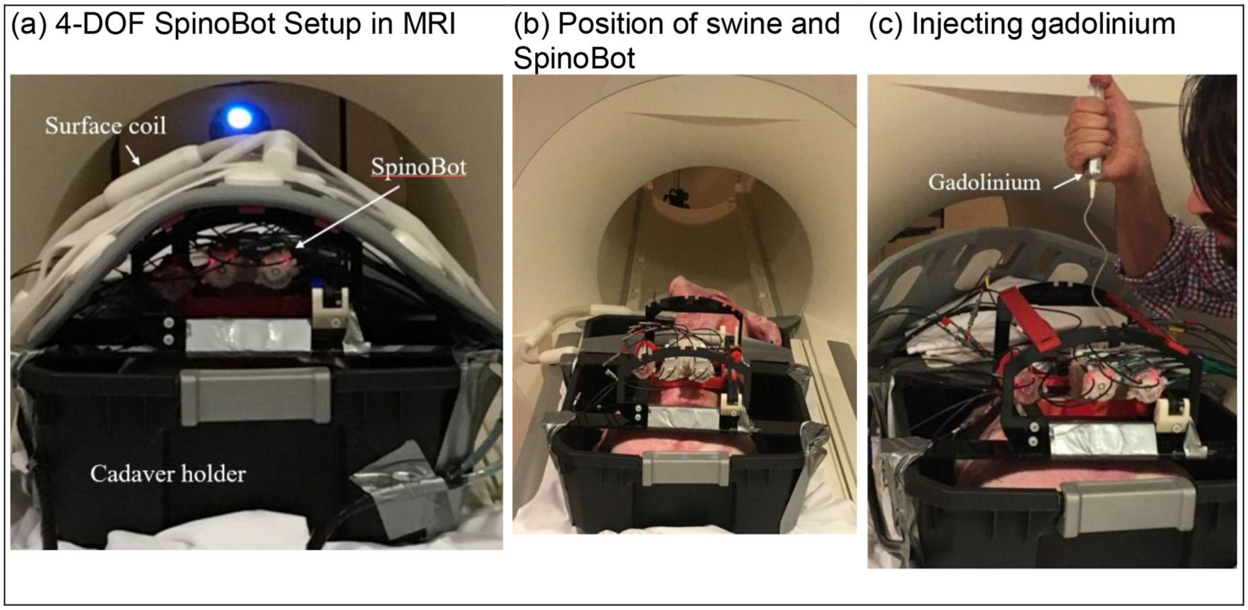

Figure 4.

Swine cadaver trials. (a) SpinoBot set up for scanning. The swine cadaver was placed in a plastic cadaver holder to avoid fluid drainage from the swine to the scanner. (b) With the surface coil removed, SpinoBot and the swine are shown. (c) After insertion of a solid needle, a hollow needle is inserted along the same path and used to inject gadolinium.

Author Manuscript Author Manuscript Author Manuscript Author Manuscript

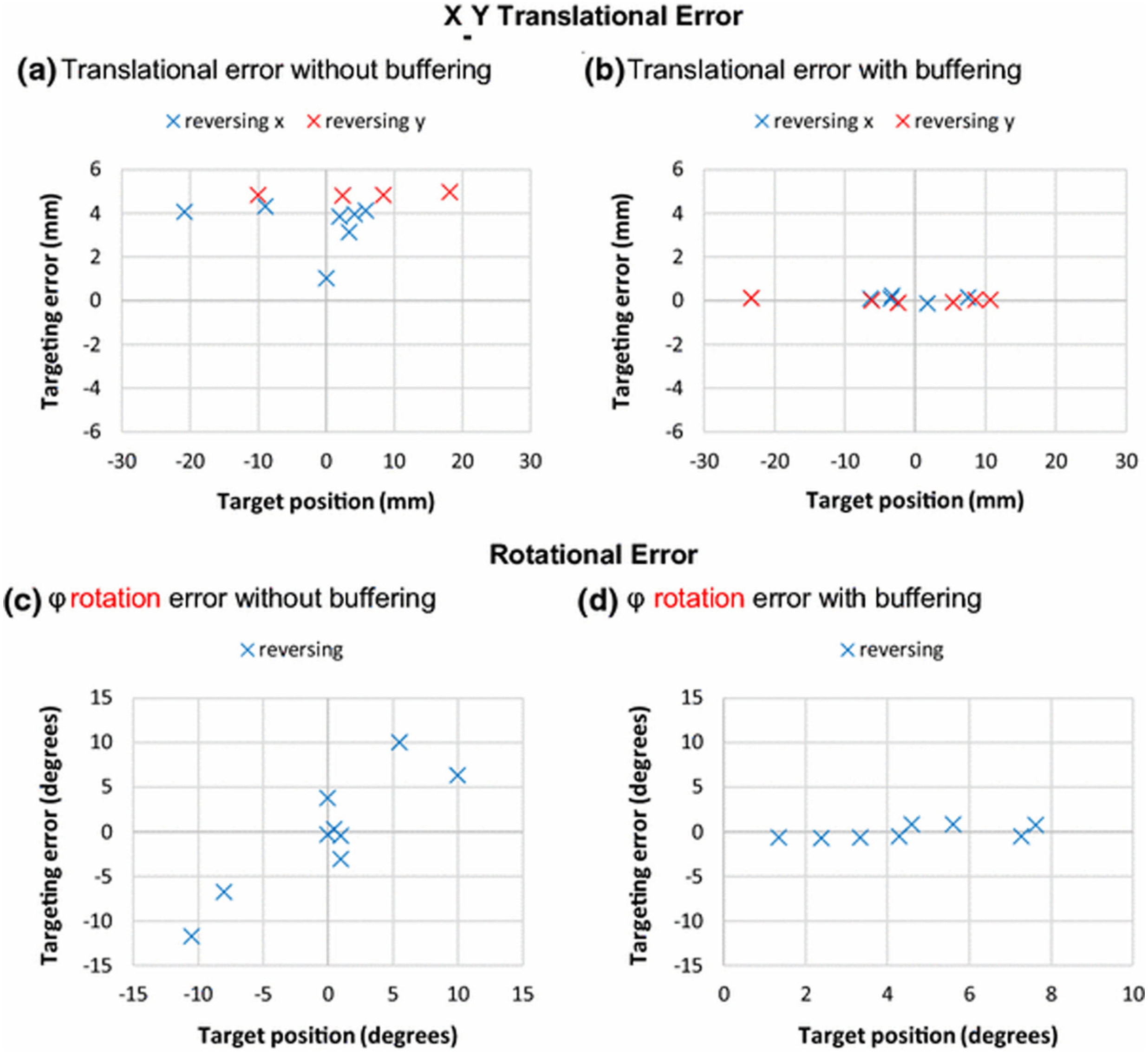

Figure 5.

Bland-Altman inspired plots visualizing the effects of implementing the buffering system. In a) and c), systematic errors without buffering of the translational and rotational axes are shown. b) and d) demonstrate negligible systematic error after implementation of the buffering. The θ rotation had similar performance as φ rotation and therefore is not shown here.

Author Manuscript Author Manuscript Author Manuscript Author Manuscript

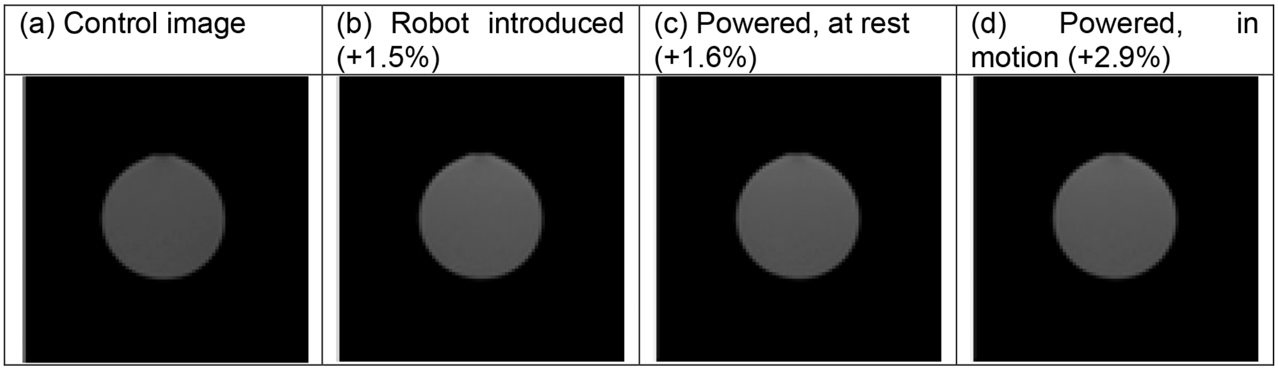
(a) Control image
(b) Robot introduced (+1.5%)
(c) Powered, at rest (+1.6%)
(d) Powered, in motion (+2.9%)

Figure 6.
True FISP MR images of the phantom obtained with the 3T MR scanner obtained under four conditions. The robot was placed immediately next to the scanned phantom.

Author Manuscript Author Manuscript Author Manuscript Author Manuscript

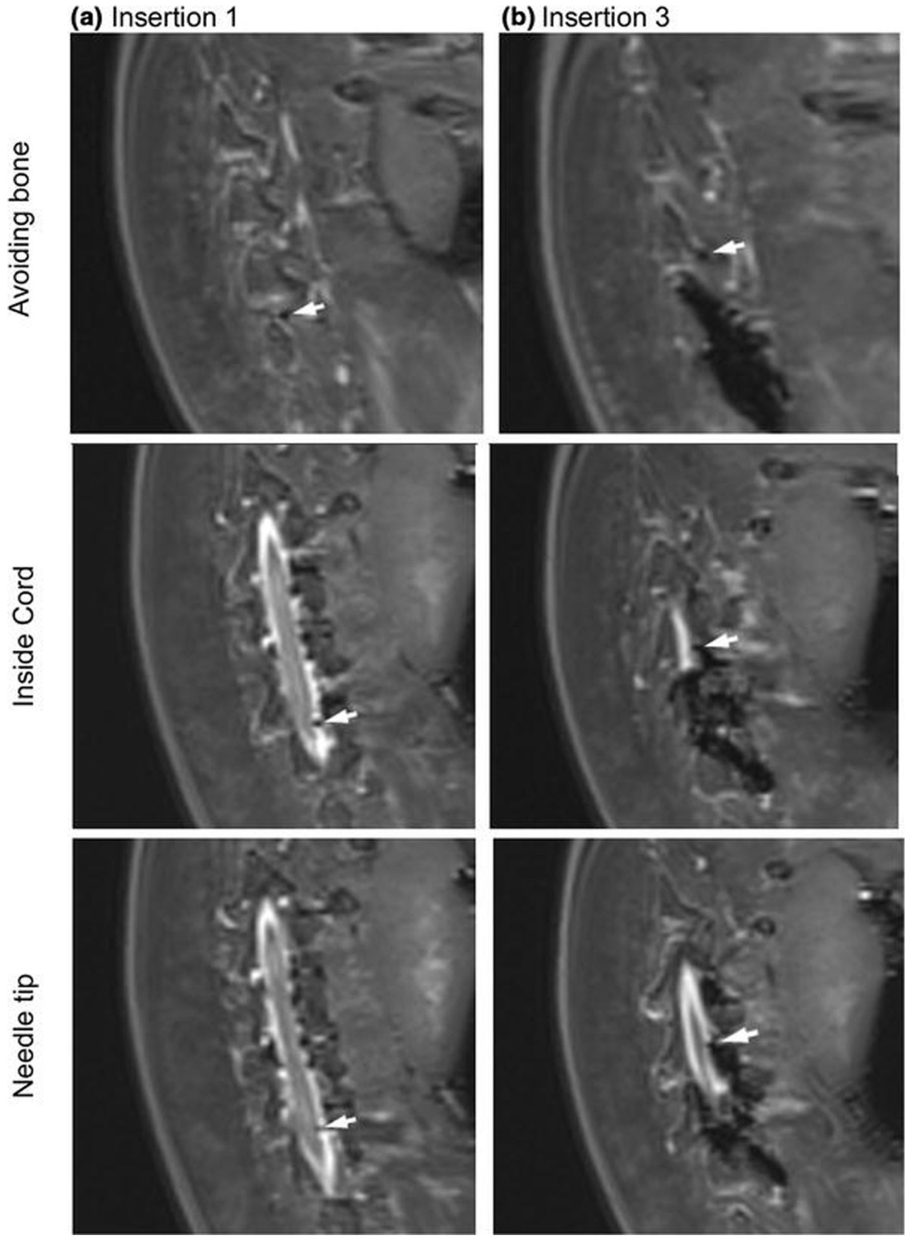

Figure 7.

MR images obtained from the cadaver trial using the 4 degree-of-freedom SpinoBot. Needle is indicated by the white arrow. Progressing from the upper images to the lower, the needle trajectory is visible as it avoids the spinous process and punctures the spine.

Author Manuscript Author Manuscript Author Manuscript Author Manuscript

Table 1.

Added value to different stakeholders through the introduction of image-guided spinal therapies using SpinoBot

Stakeholder	Outcome	Value Added
Patients	Patients permitted for more advanced and complex treatments for ALS	Shortened procedure time Improved quality of life
Surgeons	Enhanced performance in surgeries which requires simultaneous use of surgical and imaging tools	Increased procedural outcomes and treatment plans Ease of use
Surgery Department	Increased patient safety and efficiency during procedures	Increasing number of patients Efficient consultation services
Hospital	Ability to take increased patient loads, follow-ups, increased procedure volume	Increased quality and efficiency and reduced cost of operations Improved patient satisfaction

Author Manuscript Author Manuscript Author Manuscript Author Manuscript

Table 2.

Design specifications

Concept	A needle (cannula and stylet) positioner and rigid guide for MRI-guided percutaneous injection into the ventral horn of the spinal cord, which requires the needle to follow a trajectory through the gaps between vertebrae[2, 3] into the spinal cord.
Size constraint	The procedure is performed in a 60–70 cm-cylinder MRI bore, where a large portion of the volume is occupied by the patient torso and abdomen, limiting the size and workspace of the robot[9, 12].
Materials	Fabrication from MR-safe materials, preferably those which do not create image-degrading magnetic susceptibility artifacts in order ensure safety and utility.
Needle	A 16-gauge cannula is necessary to allow a needle from a microinjection system to be used, as well as ensuring sufficient strength and stiffness to pierce muscle and lamina.
Insertion	Needle insertions are performed by hand in order to obtain realistic force feedback.
Method of attachment	The method with which the device is mounted to the patient must be minimally invasive. The device should require minimal adjustment after it has been positioned on the patient.
Clinical requirement	Must be disposable or able to be sterilized for future in-vivo trials.
Procedure length	Use of device should shorten procedure (typical length of direct injection procedure is 4 hours).
Function	Allow physician to perform multiple insertions along an approximately 10 cm length of the spinal cord without adjusting fixation to the patient, which reduces procedure time.
Range of motion	**1** Allow manipulation of the needle orientation and position by providing: **a.** 2-DOF needle translations (90 mm in left-to-right direction, and 140 mm in head-to-foot direction relative to patient orientation) **b.** 2-DOF needle rotations (±30° left-to-right rotation, ±35° head-to-foot rotation relative to patient orientation) **2** Provide rigid support for needle during manual 1-DOF needle insertion.
Targeting accuracy (angle)	2°
Targeting accuracy (position)	2.5 mm

Author Manuscript Author Manuscript Author Manuscript Author Manuscript

Table 3.

Robot components and specifications

No.	Part	Description	Parameters
0	robot	4 DOF with optimal workspace for spinal targeting. Pneumatically activated, optically encoded.	Length = 310 mm Width = 240 mm Height = 50 mm
1	coil support	Supports the imaging coils.	Height = 110 mm
2	x-axis actuator	Provides movement in the X direction (left-to-right direction relative to patient orientation). Actuator connected to gearbox. Pneumatically actuated motor with stepdown gear. Non-backdrivable. Motor mounted on translating stage (4); moves the angulation stage (7). Timing belt is the driving mechanism.	Force = 11.7 N Range of motion = 90 mm
3	y-axis actuator	Provides movement in the Y direction (head-to-foot direction relative to patient orientation). Actuator connected to gearbox. Pneumatically actuated motor with stepdown gear. Non-backdrivable. Motor mounted on coil support (1); moves the translating stage (4). Timing belt is the driving mechanism.	Force = 11.7 N Range of motion = 140 mm
4	translating stage	Driven by the Y-axis actuator (3) in the Y direction. X-axis actuator mounted on translating stage moves angulation stage in X direction. Overall, acts as intermediate stage constraining the angulation stage.	X direction travel length = 90 mm Y direction travel length = 140 mm
5,6	angulation actuators	Pneumatically powered motors connected to stepdown gearbox, driving the angulation stage (7), allowing the movement of (8) theta angulation unit which provides head-to-foot rotation (θ) and (9) phi angulation unit which provides left-to-right rotation (φ).	θ rotation: Torque = 1.03 Nm Speed = 2.43 degrees/sec φ rotation: Torque = 0.41 Nm Speed = 6.08 degrees/sec
7	angulation stage	Inside angulation stage are θ and φ angulation units (8) and (9). Timing belts are used to connect (5) and (6) to (8) and (9).	2 DOF
8	theta (θ) angulation unit	Drives the needle guide in the theta direction (θ), as described in Fig. 2. Theta direction is the rotation about the left-to-right axis (which results in head-to-foot rotation).	θ = ±35°
9	phi (φ) angulation unit	Drives the needle guide in the phi direction, as described in Fig. 2. Phi direction is the rotation about the head-to-foot axis (which results in left-to-right rotation).	φ = ±30°
10	needle insertion guide	Needle channel guides the needle to the target in the spinal cord. Driven by (8) and (9) in theta and phi directions.	Insertion depth of 0 to 20 cm below robot
11	image contrast	Diluted gadolinium imaging agent produces visible brightness in MR images, marking the position of the needle insertion guide (10).	Diluted gadolinium

Author Manuscript

Author Manuscript

Author Manuscript

Author Manuscript

Table 4 –

Workflow & procedural time for MRI-guided spinal cord injections

Step	Description	Time
1. Robot Setup	Setting up the robot and control unit in the scanner and control rooms	10 min.
2. Patient/robot Preparation	Locating subject on the scanner table, and mounting the robot on the spine of the scan subject.	20 min.
3. Initial Scans	Localizing scans and high-resolution volumetric images of target anatomy	15 min.
4. Registration	Registering the robot to the MRI coordinate using fiducial markers	2 min
5. Planning	Choice of target and needle path points by operator	2 min.
6. Positioning & Insertion	Relocation of the needle guide to the target point. Needle insertion into the spinal cord with gadolinium injection.	5 min.
7. Confirmation	Confirmation scan to verify final tip position	5 min.
8. New Target	Repeating Steps 5–7	10 min.
	Total:	59+ min.